On the Generality of Molecular Volcano Plots

Dr. Matthew D. Wodrich,[a] Boodsarin Sawatlon,[a,b] Dr. Michael Busch,[a,b,c] and Prof. Dr. Clémence Corminboeuf[a,b]*

[a]Laboratory for Computational Molecular Design, Institute of Chemical Sciences and Engineering, Ecole Polytechnique Fédérale de Lausanne, 1015 Lausanne, Switzerland

[b]National Centre for Computational Design and Discovery of Novel Materials (MARVEL), Ecole Polytechnique Fédérale de Lausanne, 1015 Lausanne, Switzerland

[c]Current Address: Department of Physics, Chalmers University of Technology, Fysikgränd 3, SE-412 96 Göteborg, Sweden

Email: clemence.corminboeuf@epfl.ch

Abstract

In homogeneous catalysis, the structure and electronic configuration of the active catalysts can vary significantly. Changes in ligation, oxidation, and spin states have the potential to strongly influence the catalytic cycle energetics that, to a large degree, dictate catalytic performance. With the increased use of computational screening strategies aimed at identifying new catalysts, ambiguity surrounding structure/electronic configurations can be problematic, since it is unclear which species should be computed to determine a catalyst's properties. Here, we show that a single volcano plot constructed from linear free energy scaling relationships is able to account for variations in ligation, oxidation, and spin state. These linear scaling relationships can also be used to predict the free energies associated with a specific structure and electronic configuration of a catalyst based on a single descriptor. As a result, a single volcano plot can be used to rapidly screen for prospective new catalysts.

Introduction

The structures of homogeneous catalysts often consist of a central metal atom surrounded by one or more ligands. This ligand environment strongly affects not only the properties and performance of a catalyst, but also influences the ultimate product and/or product ratio.[1] In the course of a reaction, a precatalyst is converted into an active catalytic species, which may involve a host of changes, including structural alterations through ligand loss,[2] redox processes that modify the oxidation state,[3] or transitions between low and high spins.[4] Computational analysis based on density functional theory has made considerable headway in deciphering the myriad energetic pathways in order to determine the true nature of the active catalyst. For instance, for Suzuki-Miyaura cross-coupling,[5] computation has revealed that existence of mono- (ML) and bisligated (ML_2) reaction pathways within the conventional low-spin Pd(0)/Pd(II) catalytic cycle (Scheme 1).[6] Experimental work points to the specific electrophile (e.g., Br) used during oxidative addition as dictating a mono- versus bisligated reaction pathway.[7] In addition, computation[6b, 6d] and experiment[2] both agree that

bulky ligands, such as Buchwald ligands,[8] favor a monoligated route. Likewise, because they readily undergo one-electron redox processes,[3, 9] nickel catalysts have access to numerous oxidation states.[10] In particular, catalytic cycles involving Ni(I)/Ni(III) [as opposed to Ni(0)/Ni(II)] species are thought to play a significant roles in some cross-coupling reactions,[11] particularly when N-heterocyclic carbenes are employed as ligands.[12]

The elusive nature of the structure and electronic configuration of the active catalyst during Suzuki-Miyaura cross-coupling arising from different ligation, oxidation, or spin states creates a challenging situation for the computational design of new catalysts. Such uncertainty imposes additional strain on how catalysts should be treated computationally in terms of: standard DFT based energetic analysis,[6b, 6c, 13] the kinetic modeling[14] of prospective mechanistic pathways, determination of theoretical turnover frequencies (*e.g.*, Shaik's energetic span model[15]), tools built to identify structure-activity relationships (*e.g.*, Sigman's multidimensional analytic tools,[16] Fey and Harvey's ligand knowledge bases,[17] and the volcano plots popularized by Nørskov[18]), and automated procedures that assess catalytic mechanisms and properties with minimal human input (*e.g.*, Wheeler's AARON,[19] the automated methods for organometallic catalysts of Martínez-Núñez,[20] Habershon's graph-based reaction path sampling,[21] as well as Maeda and Morokuma's artificial force induced reactions,[22] which have now been applied to catalysis[23]).

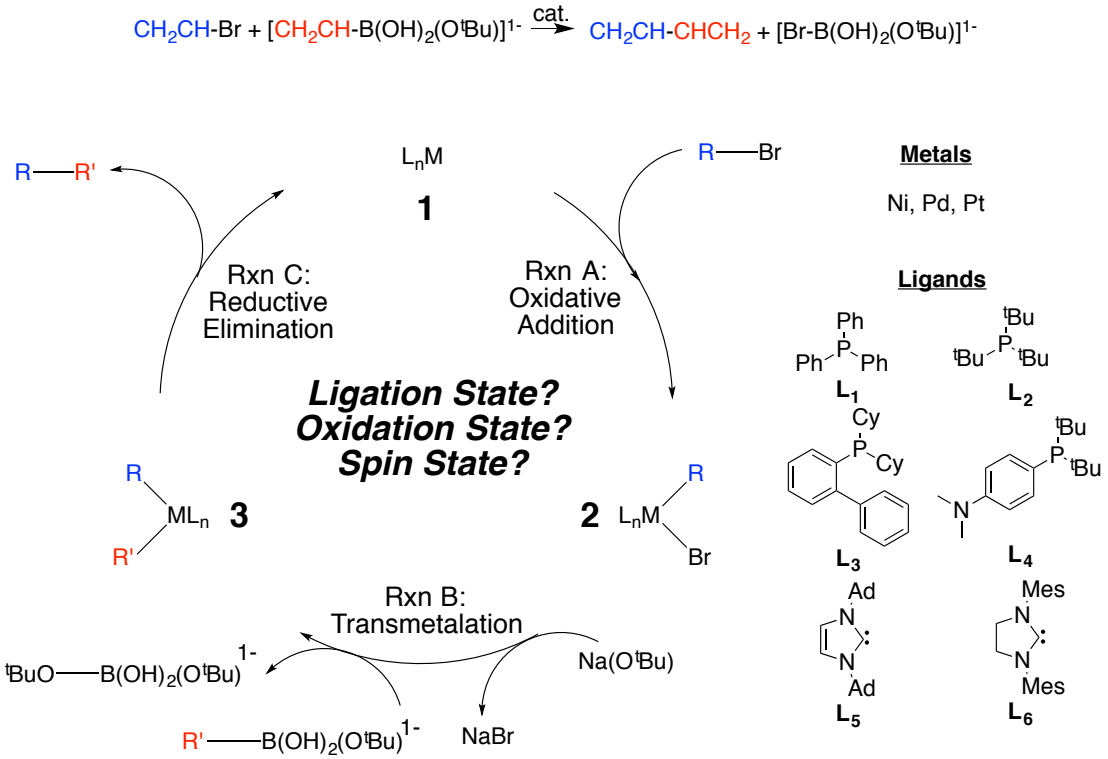

Scheme 1. The Suzuki-Miyaura cross-coupling reaction being studied (top), reaction mechanism indicated potential alternatives to the depicted pathway (left), along with metal and ligands used to create linear free energy scaling relationships and volcano plots (right).

Recently, our group began using molecular volcano plots,[24] a counterpart to the ubiquitous volcano plots advocated by Nørskov[18] for heterogeneous and electrocatalytic applications, to analyze reactions involving homogeneous catalysts.[25] Built upon linear free energy scaling relationships (LFESRs),[26] these plots relate a descriptor variable with a catalyst's intrinsic properties, such as a thermodynamic or kinetic free energy profile. Assuming an easily computed descriptor variable, volcano plots become powerful tools for rapidly screening prospective new catalytic species via structure-activity type relationships. In order to provide a comprehensive picture of homogenous catalytic species, it is essential that these molecular volcano plots are sufficiently flexible to account for changes brought about by different ligation, oxidation, or spin states, yet accurate enough to provide useful energetic information about the individual catalysts.[27] The purpose of this contribution is to gauge the

influence that alterations to the structure (via examination of different ligation states) and electronic configuration (via examination of different spin and oxidation states) of the active catalysts have on the construction of linear free energy scaling relationships and thermodynamic volcano plots. This objective is accomplished by examining the Suzuki-Miyaura cross-coupling reaction depicted in Scheme 1.

Results and Discussion

Linear Free Energy Scaling Relationships. A central concept underpinning volcano plots are that the free energies of the steps of the catalytic cycle do not vary freely, but are related to one another through linear free energy scaling relationships (LFESRs). Once these relationships are established, the free energy of any individual reaction step can be estimated by knowing the value of the "descriptor variable." Previously, we found the free energy associated with oxidative addition [ΔG(Rxn A), Scheme 1, which is equivalent to ΔG_{RRS}(**2**) as defined in Equation 1], to be an excellent descriptor.[25a, 25c, 25d] Figure 1 shows the LFESRs, as determined by DFT computations (see Computational Details), which relate the stabilities of catalytic cycle intermediates **2** and **3** (see Scheme 1, stabilities defined by Equations 1 and 2) to one another. Figure 1a, which depicts the scaling relationship for 18 bisligated catalysts (combinations of the three metals and six ligands depicted in Scheme 1), reveals a strong correlation where knowing the value of ΔG_{RRS}(**2**) (our chosen descriptor variable) leads to a very good estimation of ΔG_{RRS}(**3**).

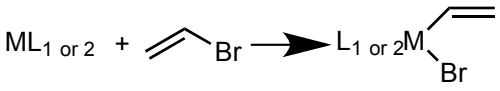

ΔG_{RRS}(**2**) Eq. 1

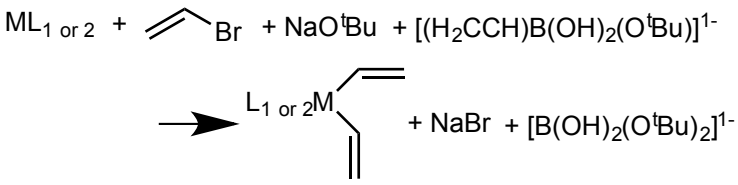

ΔG_{RRS}(**3**) Eq. 2

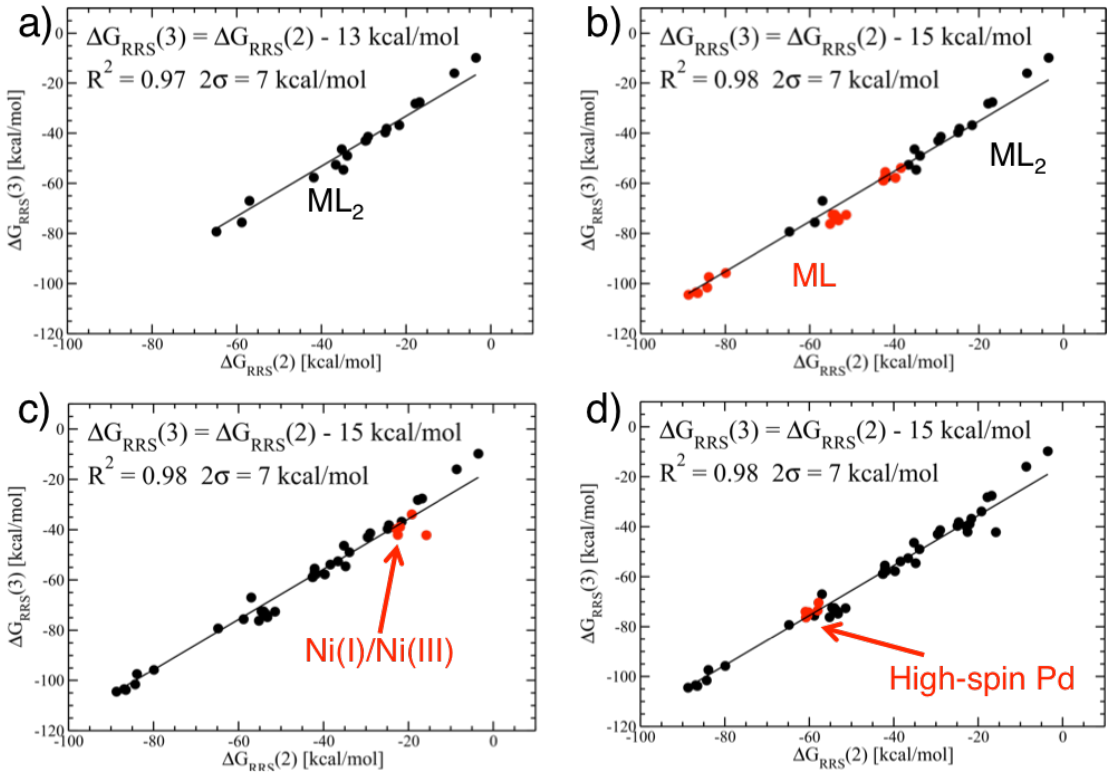

Figure 1. Linear free energy scaling relationships between the binding energies of **2** [ΔG_{RRS}(**2**)] and **3** [ΔG_{RRS}(**3**)] as defined by equations 1 and 2 for (a) the 18 bisligated catalysts, (b) the 18 bisligated from figure 1a (black) plus 18 monoligated catalysts (red), (c) the 36 catalysts from figure 1b (black) plus six monoligated Ni catalysts with Ni(I)/Ni(III) oxidation states (red), and (d) the 42 catalysts from figure 1c (black) plus six high-spin monoligated Pd catalysts (red). All catalysts depicted in (a) and (b) were computed as closed-shell singlet species. The Ni(I)/Ni(III) catalysts in (c) were computed as doublet cations and the high-spin Pd catalysts in (d) were computed as neutral triplets.

Of critical importance is how a change in ligation state affects the LFESRs. Two potential scenarios exist: either the bis- and monoligated catalysts are described by two unique sets of LFESRs or they are governed by the same set of scaling relationships. For the first case, it would be necessary to construct two volcano plots, one of which would identify

bisligated catalysts with appealing thermodynamic profiles while a second would accomplish the same objective for monoligated species. In fact, Figure 1b shows the 18 monoligated variants of the original set of catalysts (red points) closely follow the LFESRs established from the bisligated species (black points), much akin to the lack of changes to scaling relationships upon geometric distortion of heterogeneous catalysts.[26, 28] Thus, there is no need to create separate volcano plots, rather, a single volcano can be constructed and individual points added for structures of the catalyst having both one and two ligands.

Intrigued to ascertain how general and robust the linear free energy scaling relationships are, we computed six monoligated nickel catalysts as doublet cations in order to ascertain the energetics of the alternative Ni(I)/Ni(III) [as opposed to Ni(0)/Ni(II)] pathway (Figure 1c). In addition, the influence of spin-state was gauged by examining six monoligated Pd catalysts with a high-spin (triplet, as opposed to singlet) electronic configuration (Figure 1d). Indeed, the same set of linear free energy scaling relationships also apply to catalysts with alternate oxidation or spin states, which is consistent with findings from heterogeneous catalysis/electrocatalysis.[26, 29] Because the LFESRs are entirely general with respect to ligation, oxidation, and spin state, a single volcano plot is able to assess the thermodynamic profiles of any prospective catalysts that follow the same reaction mechanism.

Molecular Volcano Plots. Having demonstrated strong linear correlations between the binding energies of **2** and **3** for each of the different variants of catalysts, we constructed a volcano plot capable of identifying those species possessing attractive thermodynamic profiles. The mathematical procedure for converting the LFESRs into volcano plots is detailed in the Supporting Information and elsewhere.[25a, 25b] The key to clearly understanding the volcano plot is grasping the meaning of the variables plotted along the x- and y-axis. The descriptor variable, ΔG(Rxn A), is given on the x-axis, and describes the strength of the catalyst/reactant interaction. The y-axis depicts the free energy needed to complete the catalytic cycle's thermodynamically most difficult reaction step (potential determining step,

pds), as defined by: $\Delta G(pds) = max[\Delta G(Rxn\ A), \Delta G(Rxn\ B), \Delta G(Rxn\ C)]$. By convention, the y-axis is plotted as the negative of ΔG(pds), meaning that positive values correspond to exothermicity. Note that the potential determining step described by the volcano plots is not identical to the rate determining step. To achieve the later, it would be necessary to compute the transition state barriers of the catalytic cycle, which is a considerably more computationally expensive, although it does provide a more accurate picture of activity of different catalyst.[25b]

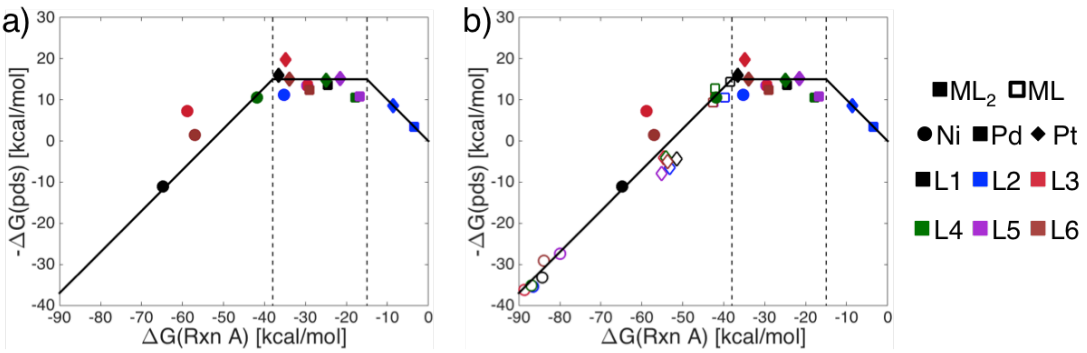

Figure 2. Volcano plots showing (a) bisligated catalysts only and (b) both bis- and monoligated catalysts. All depicted catalysts were computed as closed shell singlets. The range of x-axis values shown are cropped to focus on the catalysts (points) discussed here. Of course, as emphasized in our earlier paper, coinage metal catalysts (see ref 25a) would be visible on the weak-binding side (right side) of the volcano. Note that the volcano plots show little functional dependence (see Figure S1).

Figure 2 shows two different volcano plots corresponding to the (a) bisligated and (b) both mono- and bisligated catalysts. The volcano plot consists of two slopes as well as a plateau region, each of which correspond to separate reaction steps (*i.e.*, oxidative addition, transmetalation, reductive elimination) being the most thermodynamically difficult step of the catalytic cycle to complete. Catalysts appearing on the "strong-binding" left slope are characterized by an overly strong catalyst/reactant interaction, which means oxidative

addition is thermodynamically very favorable and reductive elimination difficult. Thus, catalysts lying in this area are limited by the free energy needed to complete reductive elimination. The opposite situation is found on the volcano's "weak-binding" right slope, where the catalyst/reactant interaction is overly weak. In this case, oxidative addition is the most thermodynamically difficult reaction step of the catalytic cycle to complete. Catalysts that lie near or on the volcano plateau have balanced thermodynamic profiles, where the catalyst/reactant interaction is neither too weak nor too strong. This means the free energies needed to complete oxidative addition and reductive elimination are roughly equivalent, and transmetalation becomes the most energetically costly reaction step of the catalytic cycle (see the Supporting Information for the free energies of each reaction step for all species). Catalysts lying in this area fulfill Sabatier's principle,[30] which states that ideal species will have a catalyst/substrate (or catalyst/reactant for homogeneous systems) interaction that is neither too weak nor too strong.

The linear scaling relationships are quite robust, and only vary slightly between different density functionals. As a result, volcano plots show little functional dependence (see Figure S1).

Evident from the comparison of the Figure 2 volcano plots is that while the ligation state of the catalysts does not influence the LFESRs, it does dramatically affect the location of the individual species on the plot. Fortunately, since a unique descriptor variable [the free energy of oxidative addition, ΔG(Rxn A)] can easily be computed for both the mono- and bisligated version of the same catalyst, the reaction energetics of both ligation states can easily be determined from the same volcano plot. Indeed, Figure 2b shows a pronounced shift toward stronger binding (*i.e.*, leftward on the x-axis) for monoligated relative to bisligated species. This stronger catalyst/reactant interaction energy likely arises from the unencumbered access of vinylbromide to the metal center during oxidative addition when only one bulky ligand is present. The similar stereoelectronic properties of the phosphine and N-heterocyclic carbene ligands tested (see Scheme 1) create clear groupings based on metal

type for the monoligated species (Figure 2b). These groupings are absent for the bisligated catalysts on account of the varying degree of access by vinylbromide to the metal center when two bulky ligands are present, which results in considerable variation in the catalyst/reactant binding energies. The location of the palladium catalysts either on the plateau or at the top of the strong-binding slope indicates that they possess favorable thermodynamic profiles in either ligation state, which aligns well with their wide ranging experimental use for cross-coupling reactions.[5b, 31] Many bisligated platinum catalysts have very good thermodynamic profiles and appear on the volcano plateau, yet, catalyst incorporating this metal are rarely used in the laboratory.[32] Indeed, the Figure 2b volcano plot shows that in their monoligated form, Pt catalysts have overly strong catalyst/reactant interactions and generally undesirable thermodynamic profiles. Because catalysts with less bulky ligands are more likely to traverse the catalytic cycle as bisligated species, increased focus in this area may lead to new viable platinum based cross-coupling catalysts.

The placement of the monoligated Ni catalysts at the bottom of the Figure 2 volcano's strong-binding side stands in stark contrast to their well-characterized experimental use.[9a] However, a great deal of evidence exists that Ni catalysts can easily access different oxidation states,[3] which may improve their thermodynamic profiles over the Ni(0)/Ni(II) cycle depicted in Figure 2b. Indeed, changing the oxidation state and establishing the thermodynamics of the Ni(I)/Ni(III) (catalysts computed as doublet cations as opposed to neutral singlets) catalytic cycle leads to a marked improvement in the thermodynamic profiles. While Ni(0)/Ni(II) species have very strong binding energies (x-axis), Figure 3 shows that the Ni(I)/Ni(III) variants are much more weakly binding (rightward shift along the x-axis) which moves the Ni catalysts onto the volcano plateau. This finding agrees very well with the myriad examples of nickel based cross-coupling catalysis present in the literature.[9a]

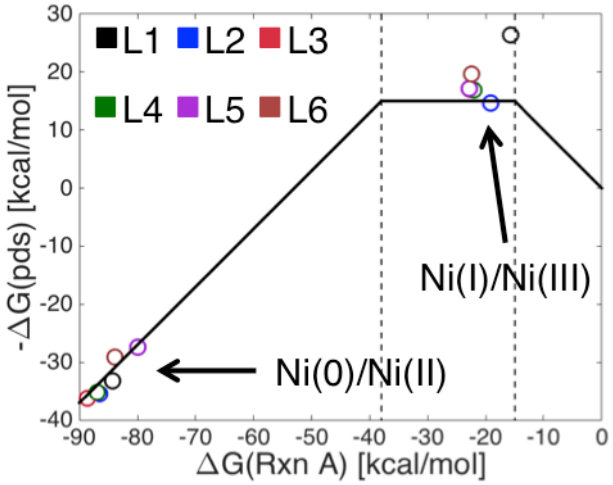

Figure 3. Volcano plot highlighting the influence of oxidation state for monoligated nickel catalysts. The Ni(0)/NI(II) were computed as closed shell neutral singlets, while the Ni(I)/Ni(III) catalysts were computed as doublet cations.

In addition to potential changes in oxidation state, the most stable electronic configuration of some catalysts may be either high-spin or low-spin. The LFESRs depicted in Figure 1 already show that high- and low-spin palladium species are governed by the same set of linear equations, which indicates that the thermodynamic profiles of both electronic configurations can be estimated using the same volcano plot. Indeed, Figure 4 shows that the higher energy monoligated triplet palladium catalysts (see Supporting Information Table S1 for relative energies) have stronger catalyst/reactant interactions than their low-spin counterparts. While the low-spin species appear very close to the volcano plateau, the enhanced binding energies of the high-spin compounds shift them further onto the strong-binding side of volcano. This equates to considerably less favorable thermodynamic profiles for the high-spin species. Nonetheless, it is important to note that while this issue of spin state may be less important for these catalysts (since the triplet species are not energetically accessible) and this specific reaction, it may be critically important for other reactions that might be examined using molecular volcano plots. In such a case, considerable care should be taken to assure that the correct spin-state for each catalyst is identified through the use of

density functionals designed to accurately reproduce the energies between different states[33] (*e.g.*, OPTX exchange[34]) or higher-level post-Hartree-Fock theoretical methods. Regardless of the specific details of correction reproducing the energy differences between spin states, the fact that a single volcano plot is able to simultaneously handle multiple spins will likely be an important point for future studies.

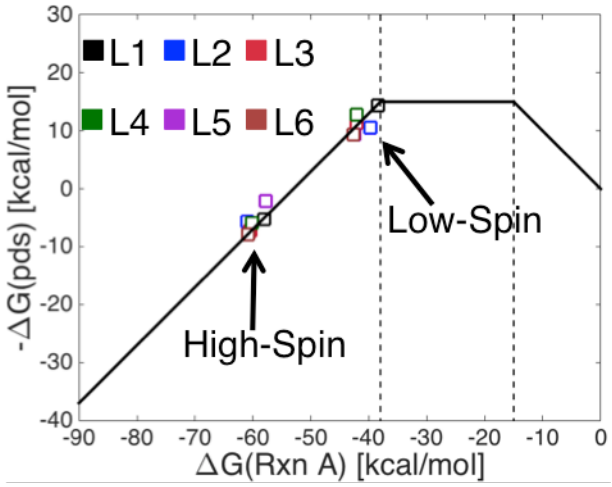

Figure 4. Volcano plot highlighting the influence of spin state for monoligated palladium catalysts. Low-spin species were computed as closed shell singlets, while high-spin species were computed as triplets.

Conclusions

In conclusion, we have shown that changes in the ligation, oxidation, and spin-states of catalysts have no influence on their underlying linear free energy scaling relationships, provided the same mechanistic pathway is followed. Because of this fact, a single volcano plot is able to provide the thermodynamic profiles of any combination of electronic, oxidation, and ligation states. The generality of both the linear scaling relationships and their corresponding volcano plots greatly simplifies the computational screening of prospective catalysts, since the thermodynamic profiles of different potential structures and electronic configurations of the active catalyst can quickly be ascertained by computing the same

descriptor variable. These findings provide critical pieces of information that improve the predictive ability of molecular volcano plots for applications in homogeneous catalysis.

Computational Methods

Geometry optimizations of all species were determined at the M06[35]/def2-SVP[36] level using the "ultrafine" integration grid (to remove known problems with grid size related to the M06 family of density functionals[37]) along with the SMD solvation model[38] (tetrahydrofuran) in Gaussian09.[39] Reported free energies include unscaled enthalpy corrections and vibrational entropy contributions only, which provides enhanced estimates of the free energies of association and dissociation processes.[6a, 40] For bisligated catalysts, structures of **2** and **3** were computed with the two phosphine/NHC ligands in their trans configuration, while monoligated catalysts used the lowest energy conformer (of R/Br – trans, R/L – trans, Br/L – trans for **2** and R/L – trans, R/R – trans for **3**). Catalysts with a M(0)/M(II) catalytic cycle were computed as neutral closed-shell singlets with the exception of the "high-spin" series of palladium catalysts, which were computed as open-shell triplets. The monoligated Ni(I)/Ni(III) catalytic cycle was computed as open-shell doublet cations. For all open-shell species, examination of the S^2 expectation values (anticipated to be 0.75 for doublets and 2.00 for triplets) revealed no contamination from higher spin states.

Acknowledgments. The National Centre of Competence in Research (NCCR) "Materials' Revolution: Computational Design and Discovery of Novel Materials (MARVEL)" of the Swiss National Science Foundation (SNSF) and the EPFL are acknowledged for financial support. Mr. Laurent Vannay and Dr. Ganna Gry'nova are acknowledged for technical support and helpful discussions.

References

[1] P. W. N. M. van Leeuwen, *Homogeneous Catalysis - Understanding the Art*, Kluwer Academic Publishers, Dodrecht, **2004**.
[2] U. Christmann, R. Vilar, *Angew. Chem., Int. Ed.* **2005**, *44*, 366-374.
[3] S. Z. Tasker, E. A. Standley, T. F. Jamison, *Nature* **2014**, *509*, 299-309.
[4] J. M. Neely, M. J. Bezdek, P. Chirik, *ACS Cent. Sci.* **2016**, *2*, 935-942.
[5] a) N. Miyaura, K. Yamada, A. Suzuki, *Tetrahedron Lett.* **1979**, *20*, 3437-3440; b) N. Miyaura, A. Suzuki, *Chem. Rev.* **1995**, *95*, 2457-2483; c) A. Suzuki, *Angew. Chem., Int. Ed.* **2011**, *50*, 6722-6737.
[6] a) A. A. C. Braga, G. Ujaque, F. Maseras, *Organometallics* **2006**, *25*, 3647-3658; b) K. C. Lam, T. B. Marder, Z. Lin, *Organometallics* **2007**, *26*, 758-760; c) C. L. McMullin, N. Fey, J. N. Harvey, *Dalton Trans.* **2014**, *43*, 13545-13556; d) M. Ahlquist, P. Fristrup, D. Tanner, P.-O. Norrby, *Organometallics* **2006**, *25*, 2066-2073.
[7] a) A. F. Littke, C. Dai, G. C. Fu, *J. Am. Chem. Soc.* **2000**, *122*, 4020-4028; b) F. Barrios-Landeros, B. P. Carrow, J. F. Hartwig, *J. Am. Chem. Soc.* **2009**, *131*, 8141-8154.
[8] R. Martin, S. L. Buchwald, *Acc. Chem. Res.* **2008**, *41*, 1561-1473.
[9] a) F.-S. Han, *Chem. Soc. Rev.* **2013**, *42*, 5270-5298; b) B. M. Rosen, K. W. Quasdorf, D. A. Wilson, N. Zhang, A.-M. Resmerita, N. K. Garg, V. Percec, *Chem. Rev.* **2011**, *111*, 1346-1416; c) N. Hazari, P. R. Melvin, M. M. Beromi, *Nat. Rev. Chem.* **2017**, *1*, 0025.
[10] J. Montgomery, in *Organometallics in Synthesis: Fourth Manual* (Ed.: B. H. Lipshutz), John Wiley & Sons, Hoboken, NJ, **2013**, pp. 319-428.
[11] a) T. J. Anderson, G. D. Jones, D. A. Vicic, *J. Am. Chem. Soc.* **2004**, *126*, 8100-8101; b) M. M. Beromi, A. Nova, D. Balcells, A. M. Brasacchio, G. W. Brudvig, L. M. Guard, N. Hazari, D. J. Vinyard, *J. Am. Chem. Soc.* **2017**, *139*, 922-936.
[12] a) K. Zhang, M. Conda-Sheridan, S. R. Cooke, J. Louie, *Organometallics* **2011**, *30*, 2546-2552; b) M. Henrion, V. Ritleng, M. J. Chetcuti, *ACS Catal.* **2015**, *5*, 1283-1302; c) I. Kalvet, Q. Guo, G. J. Tizzard, F. Schoenebeck, *ACS Catal.* **2017**, *7*, 2126-2132.
[13] a) L. J. Gooßen, D. Koley, H. L. Hermann, W. Thiel, *Chem. Commun.* **2004**, 2141-2143; b) L. J. Goossen, D. Koley, H. L. Hermann, W. Thiel, *Organometallics* **2005**, *24*, 2398-2410; c) A. A. C. Braga, N. H. Morgon, G. Ujaque, F. Maseras, *J. Am. Chem. Soc.* **2005**, *127*, 9298-9307; d) A. A. C. Braga, N. H. Morgon, G. Ujaque, A. Lledós, F. Maseras, *J. Organomet. Chem.* **2006**, *691*, 4459-4466; e) C. Sicre, A. A. C. Braga, F. Maseras, M. M. Cid, *Tetrahedron* **2008**, *64*, 7437-7443; f) M. Pérez-Rodríguez, A. A. C. Braga, M. Garcia-Melchor, M. H. Pérez-Temprano, J. A. Casares, G. Ujaque, A. R. de Lera, R. Álvarez, F. Maseras, P. Espinet, *J. Am. Chem. Soc.* **2009**, *131*, 3650-3657; g) J. Jover, N. Fey, M. Purdie, G. C. Lloyd-Jones, J. N. Harvey, *J. Mol. Catal. A* **2010**, *324*, 39-47; h) C.-M. Weng, F.-E. Hong, *Dalton Trans.* **2011**, *40*, 6458-6468; i) M. A. Ortuño, A. Lledós, F. Maseras, G. Ujaque, *ChemCatChem* **2014**, *6*, 3132-3138.
[14] C. L. McMullin, J. Jover, J. N. Harvey, N. Fey, *Dalton Trans.* **2010**, *39*, 10833-10836.
[15] a) S. Kozuch, S. Shaik, *J. Am. Chem. Soc.* **2006**, *128*, 3355-3365; b) S. Kozuch, S. Shaik, *J. Phys. Chem. A* **2008**, *112*, 6032-6041; c) S. Kozuch, S. Shaik, *Acc. Chem. Res.* **2011**, *44*, 101-110.
[16] a) K. C. Harper, M. S. Sigman, *Proc. Natl. Acad. Sci. U.S.A.* **2011**, *108*, 2179-2183; b) K. C. Harper, M. S. Sigman, *Science* **2011**, *333*, 1875-1878; c) K. C. Harper, E. N. Bess, M. S. Sigman, *Nat. Chem.* **2012**, *4*, 366-374; d) K. C. Harper, S. C. Vilardi, M. S. Sigman, *J. Am. Chem. Soc.* **2013**, *135*, 2482-2485; e) A. Milo, A. J. Neel, F. D. Toste, M. S. Sigman, *Science* **2015**, *347*, 737-743; f) Z. L. Niemeyer, A. Milo, D. P.

Hickey, M. S. Sigman, *Nat. Chem.* **2016**, *8*, 610-617; g) M. S. Sigman, K. C. Harper, E. N. Bess, A. Milo, *Acc. Chem. Res.* **2016**, *49*, 1292-1301.

[17] a) N. Fey, A. C. Tsipis, S. E. Harris, J. N. Harvey, A. G. Orpen, R. A. Mansson, *Chem. Eur. J.* **2006**, *12*, 291-302; b) N. Fey, J. N. Harvey, G. C. Lloyd-Jones, P. Murray, A. G. Orpen, R. Osborne, M. Purdie, *Organometallics* **2008**, *27*, 1372-1383; c) N. Fey, M. F. Haddow, J. N. Harvey, C. L. McMullin, A. G. Orpen, *Dalton Trans.* **2009**, 8183-8196; d) N. Fey, A. G. Orpen, J. N. Harvey, *Coord. Chem. Rev.* **2009**, *253*, 704-722; e) J. Jover, N. Fey, J. N. Harvey, G. C. Lloyd-Jones, A. G. Orpen, G. J. J. Owen-Smith, P. Murray, D. R. J. Hose, R. Osborne, M. Purdie, *Organometallics* **2010**, *29*, 6245-6258; f) J. Jover, N. Fey, J. N. Harvey, G. C. Lloyd-Jones, A. G. Orpen, G. J. J. Owen-Smith, P. Murray, D. R. J. Hose, R. Osborne, M. Purdie, *Organometallics* **2012**, *31*, 5302-5306.

[18] a) J. K. Nørskov, T. Bligaard, J. Rossmeisl, C. H. Christensen, *Nat. Chem.* **2009**, *1*, 37-46; b) A. J. Medford, A. Vojvodic, J. S. Hummelshøj, J. Voss, F. Abild-Pedersen, F. Studt, T. Bligaard, A. Nilsson, J. K. Nørskov, *J. Catal.* **2015**, *328*, 36-42; c) Z. W. Seh, J. Kibsgaard, C. F. Dickens, I. Chorkendorff, J. K. Nørskov, T. F. Jaramillo, *Science* **2017**, *355*, eaad4998.

[19] a) B. J. Rooks, M. R. Haas, D. Sepúlveda, T. Lu, S. E. Wheeler, *ACS Catal.* **2015**, *5*, 272-280; b) A. C. Doney, B. J. Rooks, T. Lu, S. E. Wheeler, *ACS Catal.* **2016**, *6*, 7948-7955; c) Y. Guan, S. E. Wheeler, *Angew. Chem., Int. Ed.* **2017**, *56*, 9101-9105.

[20] a) E. Martínez-Núñez, *J. Comput. Chem.* **2015**, *36*, 222-234; b) J. A. Varela, S. A. Vázquez, E. Martínez-Núñez, *Chem. Sci.* **2017**, *8*, 3843-3851.

[21] a) S. Habershon, *J. Chem. Phys.* **2015**, *143*, 094106; b) S. Habershon, *J. Chem. Theory Comput.* **2016**, *12*, 1786-1798.

[22] a) S. Maeda, K. Morokuma, *J. Chem. Phys.* **2010**, *132*, 241102; b) S. Maeda, K. Ohno, K. Morokuma, *Phys. Chem. Chem. Phys.* **2013**, *15*, 3683-3701; c) S. Maeda, T. Taketsugu, K. Morokuma, *J. Comput. Chem.* **2014**, *35*, 166-173.

[23] T. Yoshimura, S. Maeda, T. Taketsugu, M. Sawamura, K. Morokuma, S. Mori, *Chem. Sci.* **2017**, *8*, 4475-4488.

[24] a) H. Gerischer, *Bull. Soc. Chim. Belg.* **1958**, *67*, 506-527; b) R. Parsons, *Trans. Faraday Soc.* **1958**, *54*, 1053-1063.

[25] a) M. Busch, M. D. Wodrich, C. Corminboeuf, *Chem. Sci.* **2015**, *6*, 6754-6761; b) M. D. Wodrich, M. Busch, C. Corminboeuf, *Chem. Sci.* **2016**, *7*, 5723-5735; c) M. Busch, M. D. Wodrich, C. Corminboeuf, *ACS Catal.* **2017**, *7*, 5643-5653; d) M. Busch, M. D. Wodrich, C. Corminboeuf, **2017**, submitted for publication.

[26] I. C. Man, H.-Y. Su, F. Calle-Vallejo, H. A. Hansen, J. I. Martínez, N. G. Inoglu, J. Kitchin, T. F. Jaramillo, J. K. Nørskov, J. Rossmeisl, *ChemCatChem* **2011**, *3*, 1159-1165.

[27] Some of the inherent shortcomings of volcano plots relate to the accuracy of both the density functional used to compute the underlying linear scaling relationships and the inherent loss in accuracy brought about by using single variable to describe all the intermediates of a catalytic cycle. Such shortcomings have been discussed within the context of heterogeneous in greater detail eslewhere, see: A. J. Medford, J. Wellendorff, A. Vojvodic, F. Studt, F. Abild-Pedersen, K. W. Jacobesen, T. Bligaard, J. K. Nørskov, Science, 2014, 345, 197.

[28] M. Busch, N. B. Halck, U. I. Kramm, S. Siahrostami, P. Krtil, J. Rossmeisl, *Nano Energy* **2016**, *29*, 126-135.

[29] M. Lehtimäki, H. Hoffmannová, O. Boytsova, Z. Bastl, M. Busch, N. B. Halck, J. Rossmeisl, P. Krtil, *Electrochim. Acta* **2016**, *191*, 452-461.

[30] a) P. Sabatier, *Ber. Deutsch. Chem. Gesellshaft* **1911**, *44*, 1984-2001; b) P. Sabatier, *La Catalyse en Chimie Organique*, Librarie Polytechnique, Paris, **1913**.

[31] a) Applied Cross-Coupling Reactions (Ed.: Y. Nishihara), Springer-Verlag, Berlin, 2013; b) Metal-Catalyzed Cross-Coupling Reactions and More, Vol. 1-3 (Eds.: A. de

Meijere, S. Brase, M. Oestreich), Wiley-VCH, Weinheim, 2014; c) New Trends in Cross-Coupling: Theory and Applications (Ed.: T. Colacot), The Royal Society of Chemistry, Cambridge, 2015; d) A. Chatterjee, T. R. Ward, *Catal. Lett.* **2016**, *146*, 820-840.

[32] A. Adhikary, H. Guan, *ACS Catal.* **2015**, *5*, 6858-6873.

[33] a) F. P. Rotzinger, *J. Chem. Theory Comput.* **2009**, *5*, 1061-1067; b) B. F. E. Curchod, F. P. Rotzinger, *Inorg. Chem.* **2011**, *50*, 8728-8740.

[34] N. C. Handy, A. J. Cohen, *Mol. Phys.* **2001**, *99*, 403-412.

[35] a) Y. Zhao, D. G. Truhlar, *Acc. Chem. Res.* **2008**, *41*, 157-167; b) Y. Zhao, D. G. Truhlar, *Theor. Chem. Acc.* **2008**, *120*, 215-241.

[36] F. Weigend, R. Ahlrichs, *Phys. Chem. Chem. Phys.* **2005**, *7*, 3297-3305.

[37] S. E. Wheeler, K. N. Houk, *J. Chem. Theory Comput.* **2010**, *6*, 395-404.

[38] A. V. Marenich, C. J. Cramer, D. G. Truhlar, *J. Phys. Chem. B* **2009**, *113*, 6378-6396.

[39] M. J. Frisch, G. W. Trucks, H. B. Schlegel, G. E. Scuseria, M. A. Robb, J. R. Cheeseman, G. Scalmani, V. Barone, B. Mennucci, G. A. Petersson, et al., Gaussian, Inc., Wallingford, CT, **2009**.

[40] a) H. Tamura, H. Yamazaki, H. Sato, S. Sakaki, *J. Am. Chem. Soc.* **2003**, *125*, 16114-16126; b) S. Sakaki, T. Takayama, M. Sumimoto, M. Sugimoto, *J. Am. Chem. Soc.* **2004**, *126*, 3332-3348; c) M. Sumimoto, N. Iwane, T. Takhama, S. Sakaki, *J. Am. Chem. Soc.* **2004**, *126*, 10457-10471.

TOC Graphic:

TOC Text: **All roads lead to**…the same volcano. Computational analysis of Suzuki-Miyaura cross-coupling reveals that changes in ligation, oxidation, and spin state of the catalyst follow the same set of linear scaling relationships. As a result, a single volcano plot can be used to estimate the thermodynamics of all prospective structural and electronic forms of a catalyst.

Keywords: Homogeneous catalysis, Density functional calculations, Transition metals, linear scaling relationships, cross-coupling